THE JOURNAL OF PHYSICAL CHEMISTRY B

ARTICLE

pubs.acs.org/JPCB

Impact Desolvation of Polymers Embedded in Nanodroplets

Si Neng Sun and Herbert M. Urbassek*

Fachbereich Physik und Forschungszentrum OPTIMAS, Universität Kaiserslautern, Erwin-Schrödinger-Straße, D-67663 Kaiserslautern, Germany

ABSTRACT: Using molecular dynamics simulation, we study the desolvation process of a polymer-loaded droplet after collision with a wall. The energy and time dependence of the process is analyzed for various droplet−polymer combinations. By changing droplet size, polymer size, solvent, and polymer species, separately, we can assess the influence of these factors individually. We find that the polymer is isolated for impact energies E per solvent molecule, which exceed a threshold value E_{isol}, which is of the order of the cohesive energy E_{coh} of the solvent. The influence of the solvent can be quantified by the solute−solvent interaction energy per molecule E_{ss}. If the same polymer is embedded in solvents with similar E_{coh}, we find that desolvation proceeds more easily in the solvent with the smaller solute−solvent interaction energy per molecule E_{ss}. Polymers with high interaction energy need higher impact energies for complete desolvation. This interface energy also characterizes the desolvation of different polymers in the same solvent. E_{isol} increases slowly with the size of the droplet and decreases with the size of the polymer. These findings may help to improve the production of intact isolated macromolecules out of their solutions.

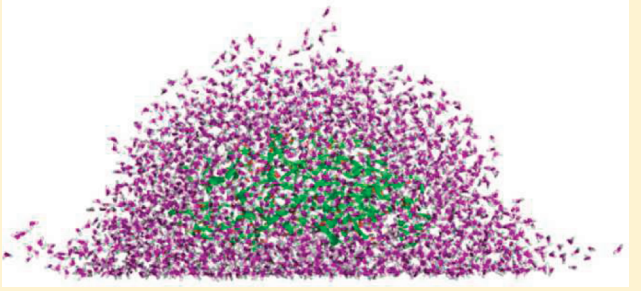

1. INTRODUCTION

A necessary prerequisite for performing mass spectrometry on macromolecules is the isolation of the macromolecule in vacuum. A common recipe for performing this task consists in solvating these molecules in an appropriate solvent, forming droplets, and eventually fully desolvating the macromolecules from the surrounding solvent. A variety of techniques have been set up for this purpose, such as electrospray ionization (ESI), matrix-assisted laser desorption (MALDI), massive cluster impact (MCI), laser spray, or laser-induced liquid beam ionization (LILBID).[1−4,3,5,6] A comparatively recent technique is *impact desolvation of electrosprayed microdroplets* (IDEM).[7] In this method, the analyte molecule is solvated in a microdroplet; the droplet is collided with a wall with the aim of desolvating the analyte without destroying it.

Evidently, the energy with which the droplet must collide with the wall has to be chosen with care. If the impact energy is too small, the droplet will not fully fragment and set the macromolecule free; if it is too large, the molecule will be heated up too strongly and may even fragment. How does the appropriate energy window depend on droplet size, on the nature of the solvent, and on the macromolecule−solvent interaction? Up to now, these questions do not appear to have been sufficiently answered.

The issue of droplet−wall collisions is of interest also in other fields of research, ranging from controlled cluster deposition[8] over surface cleaning by cluster impact[9] to cluster-impact chemistry.[10] The fragmentation of pure droplets (without embedded macromolecules) has been studied previously for clusters composed of van der Waals-bonded atoms[11−14] and molecules[15,16] and, in particular, also for water.[17−19] The collision of a protein-loaded droplet with a wall has only rarely been studied before.[20]

We employ molecular dynamics simulations on model systems to obtain a deeper understanding of these questions. We choose a particularly simple macromolecule, a polymer, and water as a common solvent; for discussing the influence of the solvent species, we also performed model simulations for Ar, as a simple example of a nonpolar fluid. By varying systematically the size of the solvent droplet and the size of the polymer, we can study the influence of these parameters on the desolvation process induced by a collision with a wall. Furthermore, by examining both a hydrophilic polymer (polyketone) and a hydrophobic polymer (polyethylene) and varying the solvent (water or Ar), we can investigate the dependence of polymer desolvation on the nature of the solvent and the solvent−polymer interaction. In addition, our analysis is able to shed light on the dynamics of the desolvation process and its dependence on impact energy.

2. METHOD

2.1. Potentials. We study two model macromolecules: polyethylene (PE), CH_3-$(CH_2)_n$−CH_3, and polyketone (PK) CH_3−$(C_2H_4COC_2H_4)_n$−CH_3. For PE, the CH_2 and CH_3 units in each monomer are considered as united atoms C* with masses of 14.027 and 15.035 amu, respectively. They are connected with neighboring C* by sp^3-type bonds. The chemical bonds within the monomers are modeled by Morse potentials both for nearest (1−2) and next-nearest (1−3) neighbors. In addition, the nonbonded intramolecular interactions are modeled by 12−6 Lennard-Jones (LJ) potentials. This model as well as the bond parameters are taken from ref 21.

Received: August 5, 2011
Revised: October 5, 2011
Published: October 08, 2011

For PK, we use a part of the OPLS (*optimized potentials for liquid simulation*) force field[22] consisting of bonding and nonbonding interactions. Although the OPLS force field is capable of considering C−H bonds explicitly, we took all $-CH_3-$ and $-CH_2-$ as united atoms in order to make the model comparable to that of PE. In this force field, the total potential energy of the polymer takes the form

$$E = \sum_{\text{bonds}} D[1 - e^{-\alpha(r - r_0)}]^2 + \sum_{\text{angles}} k_\theta(\theta - \theta_{\text{eq}})^2 + \frac{1}{2}\sum_{ij}\left\{4\varepsilon_{ij}\left[\left(\frac{\sigma_{ij}}{r_{ij}}\right)^{12} - \left(\frac{\sigma_{ij}}{r_{ij}}\right)^{6}\right] + \frac{q_i q_j e^2}{4\pi\varepsilon_0 r_{ij}}\right\} \quad (1)$$

The Morse potentials for direct-neighbor C−C bond stretching has parameters $\alpha = 21.93\ \text{nm}^{-1}$, $r_0 = 1.53$ Å, and $D = 3.6192$ eV,[23] where α has been determined from the spring constant given in GROMACS. All further parameters were directly taken from the GROMACS-4.0 package.[23] In our PK model, each ketone monomer is followed by two ethylene monomers. Charges are only on the C and O atoms in the polarized ketone monomers and assume values of $+0.47e$ for C and $-0.47e$ for O. The LJ interaction acts only between these atoms in the ketone group as well as between the CH_2 and CH_3 groups.

We mainly employ water as a solvent due to its importance in practice. However, we also studied the solvent Ar as a model for a nonpolar solvent. The TIP4P model of water[24] is employed because it shows relatively good ability in describing the phase transitions of water.[25] In this model the charges on the H atoms are $+0.52e$, while the O−O LJ bond strength is $\varepsilon = 6.72$ meV. The potential for argon is taken from ref 26. The polymer−solvent interaction is mediated by the nonbonding (van der Waals and electrostatic) terms in the interaction, as described in eq 1, and in the corresponding terms of the TIP4P or Ar potential. The LJ parameters for the interaction between water and polymer atoms are again provided by GROMACS;[23] the LJ strength between the O of a water molecule and a CH_2 group on the polymer is $\varepsilon = 6.41$ meV; other LJ interactions are of similar strength. Note that for hydrophobic polymers such as PE, the electrostatic interaction E_{el} is zero, while for hydrophilic polymers such as PK, E_{el} will provide a relatively strong interaction between polymer and solvent molecules.

We note that our water potential is rigid and does not allow for vibrational excitation; the polymer model of course allows for vibrations. Due to the high energy of the vibrational quanta of water (at 0.2 eV for the bending mode and 0.45 eV for the stretch modes), this is a good approximation for the smaller impact energies, but becomes more critical at higher energies. We give the following arguments that vibrational excitation will not change the results strongly. Polymer isolation occurs for impact energies around $(0.5-1.3)\ E_{\text{coh}}$, see Figure 5. At these energies, the maximum water temperature is only around 1000 K, where vibrational excitation (in thermal equilibrium) can be neglected. If vibrational excitation does occur during the strongly nonequilibrium collision with the wall, the excitation is be quickly quenched, on time scales <1 ps.[27,28] However, we note that a previous simulational study of the scattering of water clusters off a repulsive surface with velocities up to 2 km/s showed that vibrational excitation does not occur directly upon impact but rather later on by coupling to the other degrees of freedom.[29]

2.2. Model Setup and Data Analysis. We describe our procedure for the case of water droplets; the procedure for Ar droplets is analogous. We prepare spherical droplets at a temperature of $T_0 = 300$ K containing a number N (between 2000 and 6000) molecules. In these, either a PK or a PE molecule is dissolved as follows. The polymer is created as a linear chain and then forced to coil up using a spherical repulsive potential.[30] After energy minimization, it is set in an cubic simulation box, which is then filled up with water. After energy minimization, a spherical droplet containing the polymer and the specified number of water molecules is cut out, heated to 300 K, and equilibrated for a few hundred ps.

The polymers contain either 298 or 604 atoms. If necessary, we specify the number of atoms in the polymer by a subscript, such as PE_{298}, for instance. These different model systems allow us to separately consider the effect of (i) droplet size, (ii) polymer size, and (iii) polymer species (hydrophilicity) on the impact dynamics and the ensuing desolvation process.

The droplets are accelerated to different impact velocities v in the range of 0.5−2.4 km/s (0.2−1.3 km/s for Ar droplets) We characterize these systems by their initial energy per molecule, E, which is composed of thermal and translational kinetic energy

$$E = \frac{6}{2}k_{\text{B}}T_0 + \frac{1}{2}mv^2 \quad (2)$$

where m is the molecular mass and k_{B} is Boltzmann's constant. Note that TIP4P water is rigid and vibrations cannot be excited. In the following we shall scale the initial energy E to the cohesive energy E_{coh} of the solvent; it is $E_{\text{coh}} = 520$ (80) meV for water (Ar). Our region of interest, where desolvation occurs, is in the range of $0.2 \le E/E_{\text{coh}} \le 2$.

While we specify the collisions by the collision energy per molecule E/E_{coh}, it may be of interest to note its velocity v and relate it to the speed of sound, which is $v_{\text{sound}} = 1.50$ km/s for liquid water at 300 K.[31] For the convenience of the reader we note that

$$v = \sqrt{\frac{E}{E_{\text{coh}}} - 0.15}\cdot 2.36\ \text{km/s} \quad (3)$$

such that the droplet has sonic speed at a collision energy of $E/E_{\text{coh}} = 0.55$.

The collision of the droplets with the wall is modeled by an external repulsive potential. Its form and parameters have been specified earlier.[15,16] This rigid-wall model appears justified at the impact velocities considered, where the wall is not damaged. Note that our impact energies are below 1 eV/molecule, which is small compared to the cohesive energy of typical wall materials. Our neglect of any adhesion between the cluster and the wall appears justified for hydrophobic wall surfaces. The droplets hit perpendicularly on the wall.

The GROMACS package[23] is used to calculate the trajectory of each molecule for 300 ps in every simulation. Our own code is used for data analysis. We quantify the droplet fragmentation using the cluster analysis presented in ref 32. It allows, in particular, to identify the *central fragment*, defined as the fragment that remains in contact with the polymer. The number of solvent molecules in the central fragment, relative to the initial number N, is denoted by f; it is the key quantity to characterize the desolvation process. $f = 0$ denotes a completely isolated macromolecule.

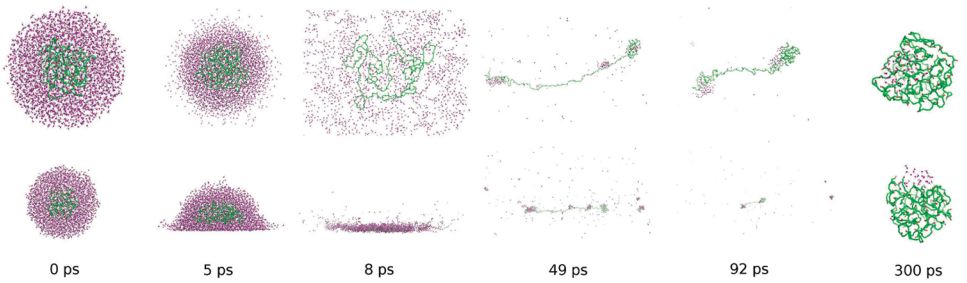

Figure 1. Snapshots of the isolation process of a PK_{604} molecule embedded in a H_2O $_{6000}$ droplet, which hits at time $t = 0$ a hard wall with energy $E/E_{coh} = 1.275$. For these parameters, the polymer does not become completely desolvated. Upper row: top view, lower row: side view. Purple: water molecules. Green: polymer (PK).

Finally, we measure the rotational (T_{rot}) and translational (T_{trans}) temperature of the solvent in the central fragment as well as the polymer temperature $T_{polymer}$, using the method described in ref 30.

3. RESULTS

Figure 1 displays a series of snapshots which show the essential stages of the collision, droplet-fragmentation and polymer-desolvation process. Time is set to $t = 0$, when the droplet starts to feel the interaction with the wall. The collision leads to a strong vertical droplet compression in the course of which the translational center-of-mass energy of the droplet is converted to internal energy. The droplet starts to spread out laterally on the surface; at these collision energies, this process has been termed "lateral jetting"[33,34,16] or "fingering".[35] This stage starts here at 5 ps and is fully developed at 8 ps. This jetting process produces small solvent clusters and monomers moving sideways along the surface with high velocity, while in the central region the system is still dense and continuous. Now, however, the high energy density inside the central region leads to a fragmentation process of the central region, during which a wide spectrum of small water clusters and molecules is formed. This stage has ended at the snapshot shown at 49 ps, where the polymer is seen to be almost completely desolvated, while a few water clusters fly away from it. Note that the polymer itself has undergone a considerable conformation change due to the violent collision process; its coiled structure has become unwound, while it slowly moves away from the surface. A similar dynamics has recently been observed in experiment.[36] In the ensuing simulation time, the polymer resumes its original coiled form, while the water on it assembles to a remaining droplet; this constitutes the *central fragment* described in section 2.2, on which our attention is focused, because its time evolution describes the desolvation process. The changes in the number of water molecules in the central droplet occurring after 49 ps are due to water evaporation.

3.1. Temporal Evolution. In order to understand quantitatively how the system is heated in the compression stage and the time evolution of the thermal energy in the simulation, the temperature evolution of polymer and solvent is shown in Figure 2a, while the evolution of the fraction f of water molecules still present in the central fragment bound to the polymer is displayed in Figure 2b. We note that the diameter of a PK_{604}-filled droplet of $N = 2000$ (6000) water molecules amounts to 5.2 (7.3) nm. An energy per molecule of $E/E_{coh} = 1.275$ was chosen, which corresponds to a supersonic velocity of $v = 2.50$ km/s. At this velocity the droplet requires a time of 2.1 (2.9) ps to cover its diameter.

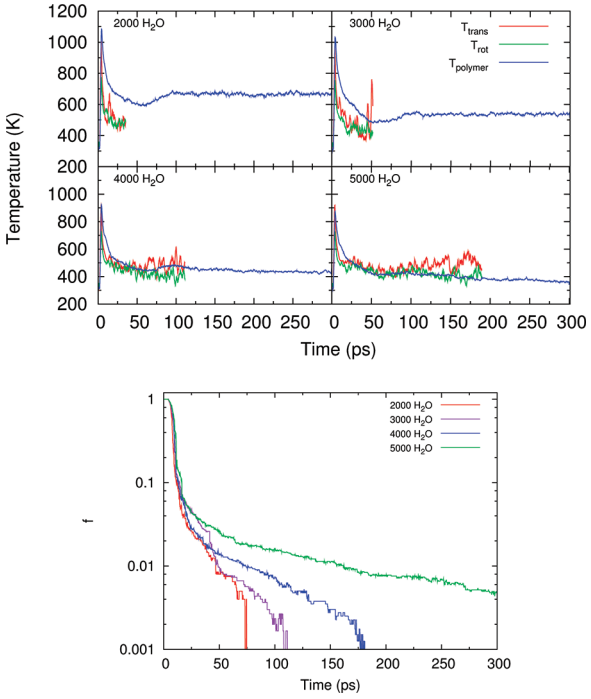

Figure 2. (Top) Time evolution of the rotational (T_{rot}) and translational (T_{trans}) temperatures of water molecules in the central fragment, and of the polymer (PK_{604}) temperature ($T_{polymer}$) after collision with a wall with energy $E/E_{coh} = 1.275$. This corresponds to a supersonic impact, compare eq 3. The initial size of the water droplet is indicated in the subfigures. Water temperatures are shown only as long as at least 30 water molecules are in the central fragment. (Bottom) Time evolution of the relative number, f, of water molecules in the central fragment.

The maximum temperature in both solvent and polymer are found at $t = 3$ ps; this marks the compression stage, during which the droplet is heated by conversion of center-of-mass energy to thermal energy. This heating process can be described in more detail on a molecular level. The sudden stopping of the front molecules by the wall lets the succeeding molecules run into them; this not only leads to a compression of the liquid but also to an increase of the pressure, since molecules are at short intermolecular distances and hence within the range of the repulsive part of the intermolecular potential. The relaxation of this pressure leads to both hydrodynamic flow and heating; the flow occurs sideways (parallel to the wall) since the direction normal to the surface is blocked by the succeeding parts of the droplet. Pressure relaxation is accompanied by energy dissipation, which

leads to heating. As Figure 2a demonstrates, both the rotational motion of the water molecules is excited and the translational temperature, that is, the random thermal motion of the molecular center-of-masses increases. The simultaneous rise of solvent and polymer temperature indicates the common and simultaneous heating of both solvent and polymer. Figure 2a also indicates that the maximum value of $T_{polymer}$ decreases with increasing droplet size, assuming values of 1100, 1020, 925, and 892 K, respectively, for increasing droplet size. The reason for this trend is as follows: The lower part of the droplet dampens the collision with the wall and transports part of the energy away by the lateral jetting process. Thus, a larger droplet provides for a softer "cushion" to dampen polymer impact onto the hard wall.

After the compression, the temperatures quickly decrease; this occurs during the lateral-jetting and multifragmentation stages described above. The initial quick decrease lasts for a time of around 20 ps. Note that here the solvent temperature is *below* that of the polymer, indicating an energy flow from the polymer to the solvent; the compression-heated polymer acts as a heat source, which is cooled by the fragmenting and evaporating solvent. During the fragmentation process, bond breaking in the solvent reduces its temperature efficiently; in an equilibrium process this would be characterized as "evaporational cooling", and in this highly nonequilibrium process, the physics is similar. Note that in this regime, rotational and translational temperature of the solvent are equal, indicating that the solvent itself is thermally equilibrated.

The later fate of the system is strongly influenced by the droplet size. The smaller droplets studied (N = 2000 and 3000) quickly desolvate the polymer. Here, after the compression stage (at t = 20 ps) so few solvent molecules remained attached to the polymer (between 60 and 270, depending on the initial droplet size, compare Figure 2b), that polymer and solvent are only in poor thermal contact; the polymer temperature is 100−200 K above that of the solvent. The strong temperature fluctuations of the solvent immediately before isolation are due to the small ensemble size. Note that the polymer temperature increases again in the time of 50−100 ps, after contact with the solvent has been lost. This temperature increase is due to conversion of polymer configurational energy to internal kinetic energy (temperature), while the polymer regains its coil structure from its strongly stretched state immediately after collision.

For the larger droplets, however (N = 4000 and 5000), good thermal equilibrium is established also in the evaporation phase. Note that here the polymer temperature continuously decreases, while the polymer is in contact with the solvent. The polymer reheating effect described above has been strongly dampened (N = 4000) or is even entirely missing (N = 5000) due to the thermal contact with the solvent. Polymer isolation occurs at 110 and 190 ps, respectively.

Complete droplet isolation occurs at 81.6, 113.7, 183.4 ps for droplet sizes of 2000, 3000, 4000 molecules; the N = 5000 droplet does not completely desolvate the polymer during the 300 ps simulation time.

3.2. Influence of Polymer Hydrophilicity. The time evolution of the relative size, f, of the central fragment also allows to characterize the influence of the nature of the polymer−solvent interaction on the desolvation process. For this purpose, we compare in Figure 3 the evolution of the desolvation of a hydrophobic PE with that of a hydrophilic PK polymer. All other parameters (droplet size N = 3000, energy E/E_{coh} = 0.5, size of polymer 298 atoms) were kept unchanged.

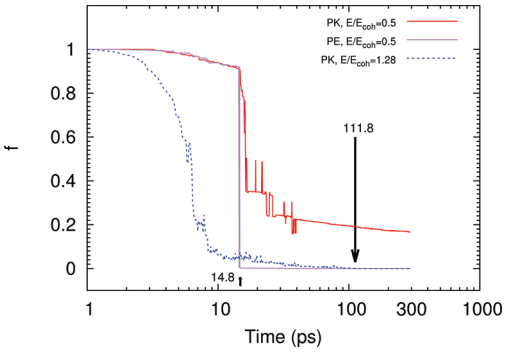

Figure 3. Time evolution of the relative number, f, of water molecules in the central fragment for PE and PK (each with 298 atoms) embedded in a $(H_2O)_{3000}$ droplet at various impact energies. The arrows denote times of isolation and are discussed in the text.

The time evolution is identical until a time of 14.8 ps, where the droplet has lost only 8% of its molecules by lateral jetting. Then the fragmentation process sets in, and instantaneously completely desolvates PE at 14.8 ps, while still around 30% of the solvent is bound to PK. At this time, the droplet has been spread out onto the wall (cf., the side view shown in Figure 1 at time 8 ps) and is torn apart laterally. The fragmentation leads to desolvation since and when the polymer−water binding forces are weaker than the water−water bonds; then the fragmenting water cloud prefers to keep bonds among themselves and loosens its bonds with the polymer. The desolvation process occurs so suddenly at this low impact energy because the expansion of the water shell is radially symmetric such that the water decouples more or less simultaneously from the polymer. In the course of time, PK sheds off more water molecules, partly in the form of larger fragments, and eventually by continuous evaporation, but at the end of the simulation 16% of the original molecules remained bound to PK, while PE already has desolvated at 14.8 ps. The "spikes" seen are due to short-lived droplet−droplet interactions in the still quite dense vapor cloud. This comparison shows clearly the decisive influence of the solvent−polymer interaction on the desolvation process.

We quantify the solvent−polymer interaction by an interaction energy E_{ss}. We calculate it by embedding the polymer in bulk solvent; after an energy minimization we determine the total solvent−polymer interaction energy by summing the respective van der Waals and electrostatic terms; E_{ss} is then obtained by dividing the total interaction energy by the number of solvent molecules within the cutoff radius (8.5 Å) of the polymer. We obtain E_{ss} = 33.45 and 15.65 meV for PK and PE, respectively, in water.

We find that PK only becomes isolated at higher impact energies, E/E_{coh} = 1.28, compare also Figure 5. We include also the time evolution of the central droplet for this high impact energy in Figure 3. Here complete isolation is achieved after 111.8 ps. Of course, due to the higher droplet impact speed, water loss occurs earlier, starting at 3 ps, with large losses due to fragmentation at 7 ps. Already at 10 ps, the central fragment only contains 6% of its initial size, and this size decreases continuously by evaporation until complete isolation.

An impact energy of E/E_{coh} = 0.5 corresponds to a subsonic velocity, 1.4 km/s (eq 3), while E/E_{coh} = 1.28 corresponds to a supersonic impact. It may hence be interesting to compare the time evolution of the temperatures of the supersonic events

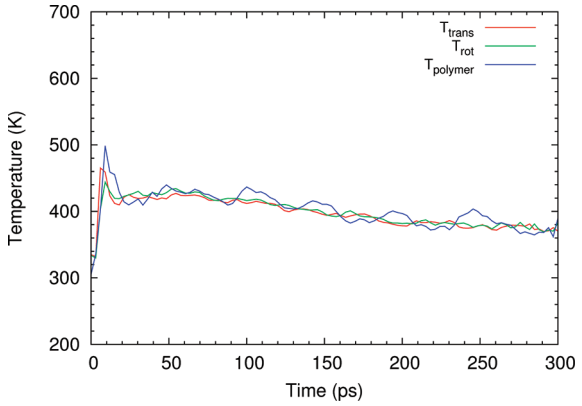

Figure 4. Time evolution of the rotational (T_{rot}) and translational (T_{trans}) temperatures of water molecules in the central fragment and of the polymer temperature ($T_{polymer}$) of a PK_{298} polymer embedded in a $(H_2O)_{3000}$ droplet after collision with a wall with energy $E/E_{coh} = 0.5$. This corresponds to a subsonic impact, compare eq 3.

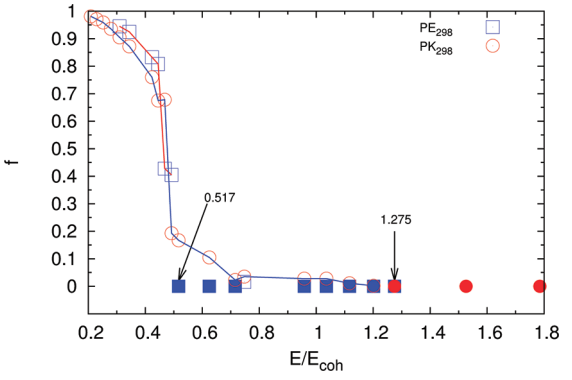

Figure 5. Dependence of the relative number, f, of water molecules in the central fragment at the end of the simulation ($t = 300$ ps) in dependence of the scaled impact energy E/E_{coh}. Initially, the droplet contained 3000 water molecules and a PK or PE polymer with 298 atoms. Filled symbols indicate $f = 0$.

shown in Figure 2 with that in the subsonic impact which we present in Figure 4. In agreement with the smaller impact energy, the temperatures attained by both water and polymer are smaller and hardly exceed 500 K. Already after around 20 ps, polymer and water are in thermal equilibrium; note that for the $N = 3000$ droplet in Figure 2, the polymer was always hotter than the water. Temperatures decrease after that time due to evaporational cooling of the water cluster.

In Figure 5, we display the dependence of the relative number, f, of water molecules in the central fragment on the impact energy E and compare droplets containing a PE and a PK polymer. While collisions with energies $\lesssim 0.4E_{coh}$ disperse the droplet only a little ($\lesssim$20% of its water molecules are lost), an increase of the impact energy to $0.5E_{coh}$ strongly shatters the droplet, such that less than 20% of the initial number of molecules remain bound to the polymer. As discussed above, the PE is then completely isolated, while the hydrophilic PK still binds water to it. From the change in slope of the $f(E)$ data, we observe that at $E/E_{coh} \cong 0.5$ the PK isolation enters a new regime, namely, the evaporation of the remaining water molecules from the PK molecule. This regime is missing for the PE molecules, because here all water molecules have been shed off the polymer during the fragmentation stage.

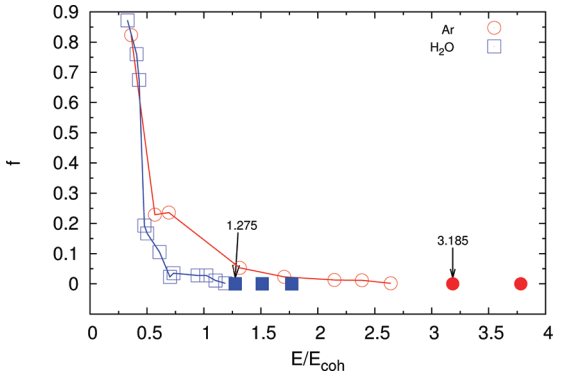

Figure 6. Dependence of the relative number, f, of solvent molecules in the central fragment at the end of the simulation ($t = 300$ ps) on the scaled impact energy E/E_{coh}. Initially the droplet contained 3000 Ar atoms or water molecules and a PK polymer with 298 atoms. Filled symbols indicate $f = 0$.

We argue that the hydrophilicity of the polymer affects only the evaporation process in the solute−solvent interface, not the fragmentation of the droplet.

3.3. Effect of Solvent. We also considered the effect of the solvent on the isolation process by dissolving the polar PK molecule in a nonpolar Ar droplet and comparing the data to those of the water droplet. The data become comparable by normalizing the impact energy to the cohesive energy of the solvent, as we proved in ref 19. PK binds H_2O molecules with strong hydrogen bonds; however, PK and Ar atoms are only bonded by the weak van der Waals interaction.

For $E/E_{coh} < 0.5$, the nature of the solvent has only little effect on the desolvation process (see Figure 6); here desolvation proceeds by the multifragmentation mechanism which is only little influenced by the polymer−solvent interface. For the final steps of desolvation, that is, to release those solvent molecules bound directly to the polymer, the nature of the interaction becomes important. As outlined above, we quantify this interaction by the solvent−solute interaction energy E_{ss}. It is $E_{ss} = 33.45$ and 8.91 meV for TIP4P water and Ar, respectively.

The data displayed in Figure 6 present what appears to be a counterintuitive information: PK is desolvated in water at smaller relative energies, $E/E_{coh} = 1.275$, than in Ar ($E/E_{coh} = 3.165$). This is of course due to the widely different values of the solvent cohesive energies, E_{coh}. When normalizing the solvent−solute interaction energy E_{ss} to E_{coh} we obtain $E_{ss}/E_{coh} = 0.064$ for water, and 0.11 for Ar; this is in agreement with the "earlier" desolvation of PK displayed in Figure 6, as compared to Ar, if energies are scaled to cohesive energies.

We conclude that the effect of the solvent on impact desolvation can to first approximation be described by its cohesive energy. In a better approximation, also the solvent−solute interaction energy enters; it is responsible for the removal of the last solvation shell, and its influence is described by the solvent−solute interaction energy E_{ss}.

3.4. Polymer Size. In order to explore the effect of polymer size on E_{isol}, we compare the desolvation of PK with 298 and 604 atoms, respectively, from a water droplet. The dependence of the relative number of solvent atoms in the central fragment on impact energy is displayed in Figure 7. We concentrate on the energy range above $E/E_{coh} = 0.5$, where the interesting physics of polymer isolation happens.

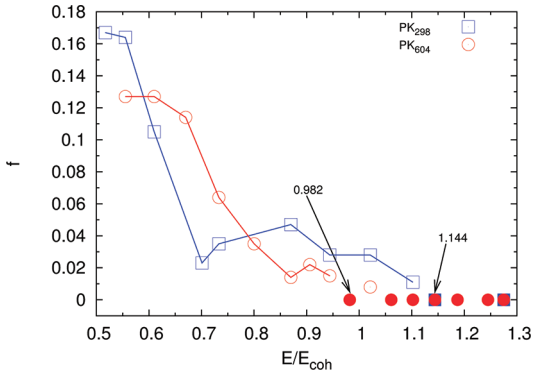

Figure 7. Dependence of the relative number, f, of water molecules in the central fragment at the end of the simulation (t = 300 ps) on the scaled impact energy E/E_{coh}. Initially the droplet contained 3000 water molecules and a PK polymer with 298 or 604 atoms. Filled symbols indicate f = 0.

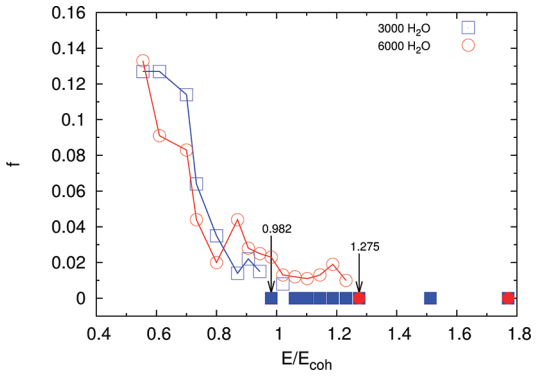

Figure 8. Dependence of the relative number, f, of water molecules in the central fragment at the end of the simulation (t = 300 ps) on the scaled impact energy E/E_{coh}. Initially the droplet contained 3000 or 6000 water molecules and a PK polymer with 298 atoms.

We find that, on average, the *smaller* polymer binds *more* solvent molecules and, consequently, has a higher isolation energy, E_{isol}/E_{coh} = 1.14 as compared to 0.98 for the larger polymer. However, the effect is not pronounced; it only amounts to 16% for a 3-fold change in polymer mass. The main reason for the easier isolation of the large polymer is the extra amount of translational energy it carries with it, and which can be used to heat and fragment the droplet and desolvate the polymer. In addition, a larger polymer can also receive more thermal energy in the collision and store it so as to reduce the evaporational cooling effect of the solvent. It might also be argued that a larger polymer will release more solvent molecules during the collision-induced unfolding process, compare Figure 1.

3.5. Droplet Size. It is known that droplet size plays only a subordinate role in the collisional fragmentation of pure, that is, not polymer-loaded droplets, see for example, refs 15 and 16. Droplets with different sizes show the same fragmentation patterns when sizes are scaled to the initial droplet size.

We compare in Figure 8 the effect of impact energy on the desolvation of a PK embedded in droplets of size 3000 and 6000 molecules. Again, we concentrate on the energy range above E/E_{coh} = 0.5, where the physics of polymer isolation happens. The differences are small in agreement with the findings for pure droplets quoted above.[15,16] However, complete polymer isolation appears to be easier in the small droplet, at E/E_{coh} = 0.982, compared to the large droplet (E/E_{coh} = 1.275).

We note that we studied in Figure 2 in detail how the polymer desolvation proceeds as a function of time for various droplet sizes, and found systematic changes. Those simulations were performed at E/E_{coh} = 1.275.

We can rationalize the dependence of polymer isolation on droplet size by the argument that, even if relative numbers f are similar at the same impact energy, absolute numbers of solvent molecules are not; and because the removal of the last solvent molecules bonded to the polymer costs thermal energy (taken from the polymer), complete isolation of a polymer embedded in a large droplet will on average require a higher impact energy. We note that, again, this is a small effect, 30%, for a doubling of the droplet size.

4. CONCLUSION

Using molecular dynamics simulation, we studied the desolvation process of a polymer-loaded droplet after collision with a wall. The energy and time dependence of the process was studied for various droplet-polymer combinations. By changing droplet size, polymer size, solvent species, and the nature of the polymer separately, the following conclusions could be obtained.

(i) The isolation process consists of two temporally consecutive phenomena, a fast (on the time scale of 10 ps) droplet multifragmentation and a slow (on a time scale of at least 100 ps) evaporation process. Our results pertain mainly to the multifragmentation process and to the early phase of the evaporation process, as long as they are contained within the 300 ps simulation time.

(ii) The polymer is isolated for impact energies E per solvent molecule, which exceed a threshold value E_{isol} that is of the order of the cohesive energy E_{coh} of the solvent. This dependence describes the prime dependence of the solvation energy on the nature of the solvent. To a better approximation, E_{isol} also depends on the size of the droplet and the polymer and the polarity of the solvent and of the polymer, as detailed below.

(iii) The solvent−polymer interaction energy E_{ss} does not affect the droplet fragmentation process; however, it can influence the evaporation of solvent molecules from the polymer−solvent interface. We thus find that, for example, a hydrophilic polymer embedded in water needs a higher impact energy E for full desolvation than a hydrophobic polymer.

(iv) Similarly, we can assess the influence of different solvents on polymer isolation. The cohesive energy of the solvent, E_{coh}, has the major influence on desolvation. If the same polymer is embedded in solvents with similar E_{coh}, we find that desolvation proceeds more easily in the solvent with the smaller solute−solvent interaction energy per molecule E_{ss}.

(v) The threshold energy for polymer isolation, E_{isol}, increases with the size of the droplet. The larger the droplet is, the more translational energy will be needed to compress the droplet, such that the polymer can reach the surface and also become compressed. We find that E_{isol} is reduced to 77% by halving the droplet size.

(vi) Larger polymers contain more translational energy that can be transferred into thermal energy and can, hence, assist the fragmentation process. Thus, E_{isol} decreases for increasing polymer size. We find that E_{isol} is reduced to 86% by doubling the polymer size.

AUTHOR INFORMATION

Corresponding Author
*E-mail: urbassek@rhrk.uni-kl.de.

ACKNOWLEDGMENT

The authors acknowledge financial support by the Deutsche Forschungsgemeinschaft via the Graduiertenkolleg 792.

REFERENCES

(1) Jarrold, M. F. *Annu. Rev. Phys. Chem.* **2000**, *51*, 179.
(2) Melchionna, S.; Briganti, G.; Londei, P.; Cammarano, P. *Phys. Rev. Lett.* **2004**, *92*, 158101.
(3) Sadeghi, M.; Wu, X.; Vertes, A. *J. Phys. Chem. B* **2001**, *105*, 2578.
(4) Sogbein, O. O.; Simmons, D. A.; Konermann, L. *J. Am. Soc. Mass Spectrom.* **2000**, *11*, 312.
(5) Patriksson, A.; Marklund, E.; van der Spoel, D. *Biochemistry* **2007**, *46*, 933.
(6) Mahoney, J. F.; Perel, J.; Ruatta, S. A.; Martino, P. A.; Husain, S.; Cook, K.; Lee, T. D. *Rapid Commun. Mass Spectrom.* **1991**, *5*, 441.
(7) Aksyonov, S. A.; Williams, P. *Rapid Commun. Mass Spectrom.* **2001**, *15*, 2001.
(8) Harbich, W. *Metal Clusters at Surfaces: Structure, Quantum Properties, Physical Chemistry*, Springer Series in Cluster Physics. Springer: Berlin, 2000; p 107.
(9) Yamada, I.; Matsuo, J.; Insepov, Z.; Aoki, T.; Seki, T.; Toyoda, N. *Nucl. Instrum. Methods Phys. Res., Sect. B* **2000**, *164−165*, 944.
(10) Christen, W.; Even, U. *J. Phys. Chem. A* **1998**, *102*, 9420.
(11) Cleveland, C. L.; Landman, U. *Science* **1992**, *257*, 355.
(12) Raz, T.; Even, U.; Levine, R. D. *J. Chem. Phys.* **1995**, *103*, 5394.
(13) Christen, W.; Even, U.; Raz, T.; Levine, R. D. *Int. J. Mass Spectrom. Ion Process.* **1998**, *174*, 35.
(14) Christen, W.; Even, U.; Raz, T.; Levine, R. D. *J. Chem. Phys.* **1998**, *108*, 10262.
(15) Zimmermann, S.; Urbassek, H. M. *Eur. Phys. J. D* **2006**, *39*, 423.
(16) Zimmermann, S.; Urbassek, H. M. *Phys. Rev. A* **2006**, *74*, 063203.
(17) Tomsic, A.; Schröder, H.; Kompa, K. L.; Gebhardt, C. R. *J. Chem. Phys.* **2003**, *119*, 6314.
(18) Tomsic, A.; Andersson, P. U.; Markovic, N.; Pettersson, J. B. C. *J. Chem. Phys.* **2003**, *119*, 4916.
(19) Sun, S. N.; Urbassek, H. M. 2011, manuscript in preparation.
(20) Thirumuruganandham, S. P.; Urbassek, H. M. *Int. J. Mass Spectrom.* **2010**, *289*, 119.
(21) Delcorte, A.; Garrison, B. J. *J. Phys. Chem. C* **2007**, *111*, 15312.
(22) Jorgensen, W. L.; Tirado-Rives, J. *Proc. Natl. Acad. Sci. U.S.A.* **2005**, *102*, 6665.
(23) van der Spoel, D.; Lindahl, E.; Hess, B.; Groenhof, G.; Mark, A. E.; Berendsen, H. J. C. *J. Comput. Chem.* **2005**, *26*, 1718.
(24) Jorgensen, W. L.; Chandrasekhar, J.; Madura, J. D.; Impey, R. W.; Klein, M. L. *J. Chem. Phys.* **1983**, *79*, 926.
(25) Vega, C.; Abascal, J. L. F.; Sanz, E.; MacDowell, L. G.; McBride, C. *J. Phys.: Condens. Matter* **2005**, *17*, S3283.
(26) Aziz, R. A. *J. Chem. Phys.* **1993**, *99*, 4518.
(27) Lock, A. J.; Bakker, H. J. *J. Chem. Phys.* **2002**, *117*, 1708.
(28) Dokter, A. M.; Woutersen, S.; Bakker, H. J. *Phys. Rev. Lett.* **2005**, *94*, 178301.
(29) Svanberg, M.; Markovic, N.; Pettersson, J. B. C. *Chem. Phys.* **1995**, *201*, 473.
(30) Sun, S. N.; Urbassek, H. M. *Appl. Phys. A: Mater. Sci. Process.* **2010**, *101*, 71–76.
(31) Lemmon, E. W.; McLinden, M. O.; Friend, D. G. In *NIST Chemistry WebBook*, NIST Standard Reference Database Number 69; Linstrom, P. J., Mallard, W. G., Eds; National Institute of Standards and Technology: Gaithersburg, MD, 20899, retrieved October 2, 2011; http://webbook.nist.gov.
(32) Stoddard, S. D. *J. Comput. Phys.* **1978**, *27*, 291.
(33) Haller, K. K.; Ventikos, Y.; Poulikakosa, D.; Monkewitz, P. *J. Appl. Phys.* **2002**, *92*, 2821.
(34) Rein, M. *Fluid Dyn. Res.* **1993**, *12*, 61.
(35) Yarin, A. L. *Annu. Rev. Fluid Mech.* **2006**, *38*, 159.
(36) Smith, M. I.; Bertola, V. *Phys. Rev. Lett.* **2010**, *104*, 154502.